Supplemental Material for "Superconductivity in Shear Strained Semiconductors"

Chang Liu(刘畅),[1,2] Xianqi Song(宋贤齐),[1] Quan Li (李全),[1,2,*]
Yanming Ma(马琰铭),[1,2,†] and Changfeng Chen(陈长风)[3,‡]

[1]*International Center for Computational Methods & Software, State Key Lab of Superhard Materials, College of Physics, Jilin University, Changchun 130012, China*
[2]*International Center of Future Science, Jilin University, Changchun 130012, China*
[3]*Department of Physics and Astronomy, University of Nevada, Las Vegas, Nevada 89154, USA*

Here we provide a systematic description of details on computational methods used in the present work and additional details supporting several results presented in the main text.

DETAILS ON COMPUTATIONAL METHODS

The first-principles energetic calculations and stress-strain relations reported in this work have been carried out using the VASP code [1], adopting the projector augmented wave (PAW) approach [2] with the valence electron configuration of s^2p^2 for both silicon and carbon, which are each described by an eight-atom unit cell. The local density approximation (LDA) has been used to describe the exchange and correlation potential between electrons as parametrized by the Ceperley and Alder functional [3]. An energy cutoff of 500 eV for Si and 800 eV for SiC and a Monkhorst-Pack grid [4] with a maximum spacing of 0.18 $Å^{-1}$ are adopted, achieving an energy convergence around 1 meV per atom with residual forces and stresses less than 0.005 eV$Å^{-1}$ and 0.1 GPa, respectively. Electronic band gaps are determined by calculations using the hybrid functional of Heyd-Scuseria-Ernzerhof (HSE) [5, 6], and the resulted band gaps for Si and SiC are 1.13 eV and 2.35 eV, respectively, which are in excellent agreement with experimental data [7, 8]. On this basis, the HSE band gaps for the deformed Si and SiC crystals are expected to provide a good description for strain induced band-gap modulations, especially the band-gap closure that signals the onset of metallization in each case.

Stress-strain relations under diverse loading conditions are calculated under a biaxial stress state that contains a shear stress and a normal compressive or tensile stress component. This approach covers the pure shear case in the limit of zero normal stress and simulates a rich variety of loading environments containing various biaxial stress states [9–11]. The shape of the deformed unit cell and atomic relaxation are determined completely at each step by the constrained structural optimization. The starting position for each strain step is taken from the relaxed coordinates of the previous strain step to ensure the quasistatic strain path, with a strain increment of 0.01 in each of the first five steps, which are in mostly linear elastic range, and then 0.005 for each subsequent steps. At each step, the applied shear strain is fixed to determine the shear stress σ_{xz}, while the other five independent components of the strain tensors and all the atoms inside the unit cell are simultaneously relaxed until the normal stress component (σ_{zz}) reaches a specified value, namely $\sigma_{zz} = \sigma_{xz}\tan\phi$ or $\sigma_{zz} = c$, where ϕ is an angular variable to adjust the ratio of the normal and shear components of the biaxial stress and c is a constant normal compressive or tensile stress. Meanwhile, all other four components of the Hellmann-Feynman stress tensor and the force on each atom become negligibly small after the full relaxation, typically less than 0.1 GPa and 0.005 eV·$Å^{-1}$, respectively. In this work, we have examined Si under diverse shear strains, including pure shear (PS), variable constrained shear (CS) with ϕ=68° corresponding to the prominent Vickers shear stress state [9–11], and constant tensile shear (TS) with c = 10 GPa, and SiC under PS stress condition.

Lattice dynamics and electron-phonon coupling behaviors have been calculated using the density-functional perturbation theory (DFPT) in linear response as implemented in the Quantum Expresso code [12], adopting a kinetic energy cutoff of 40 Ry and 70 Ry for Si and SiC, respectively. A k-mesh of 16×16×24 was used for the electronic calculations and a 4×4×6 q-mesh for the lattice dynamics calculations to achieve good convergence. Dynamic stability of deformed crystals was determined by checking for the absence of imaginary phonon modes, and the electron-phonon coupling (EPC) behaviors were evaluated and superconductivity assessed up to the highest strain for the dynamically stable structure on each chosen deformation path.

Phonon calculations in this work are performed without considering anharmonic effects. The stress-strain curves are determined by quasistatic structural optimization following the standard procedure, where stress is calculated by taking the derivative of the energy of the strained crystal with respect to strain. Phonon calculations within the harmonic approximation are subsequently performed to check the dynamic stability along specific deformation paths. Anharmonic effects could influence the dynamic stability of the deformed structure, thus affect the stable strain range of the stress-strain curve. It is noted, however, that anharmonicity is appreciable at high temperatures [13]. In this work, the superconducting states of deformed Si and SiC emerge at very low temperatures (below 10 K) and, therefore, no significant anharmonicity is expected. Moreover, re-

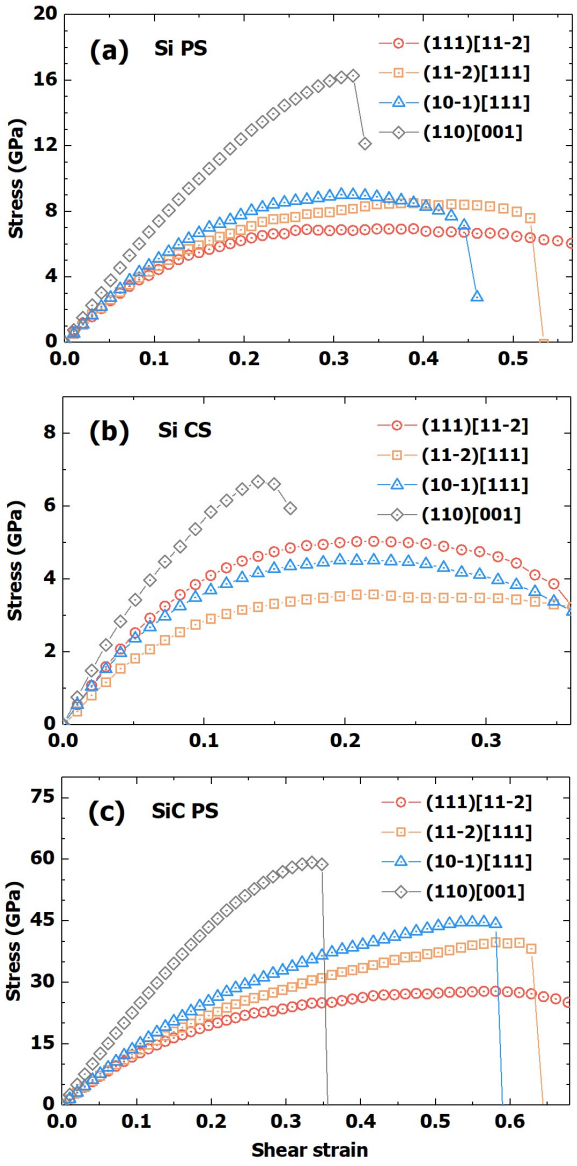

FIG. S1: Stress response under various shear-strain conditions. (a) Si under pure shear (PS), (b) Si under constrained shear (CS) and (c) SiC under PS strains. Specific shear slip directions are listed in each panel, and the most flattened curves, i.e., Si PS (111)[11-2], Si CS (11-2)[111] and SiC PS (111)[11-2], which represent the most favorable cases for metallization, are selected as shown in the main text. Covalent solids like diamond and Si host strongly directional bonding configurations, generating highly anisotropic stress responses. In this work, our goal is to explore strain-induced metallic and superconducting structure in Si; we therefore have mostly focused on stress responses along the (111)[11-2] PS and several closely related deformation paths. For comparison, we also show the shear-strain curve under the (110)[001] PS strain that exhibits a steeper rise of stress, which is commonly seen in covalent solids.

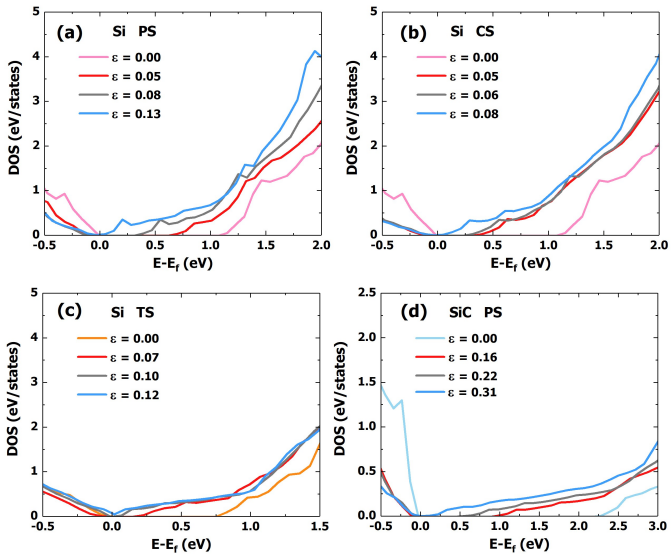

FIG. S2: Electronic band gap from HSE calculations under various shear-strain conditions. (a) Si PS (111)[11-2], (b) Si CS (11-2)[111], (c) Si TS (111)[11-2], (d) SiC PS (111)[11-2]. Results at selected strain points are shown.

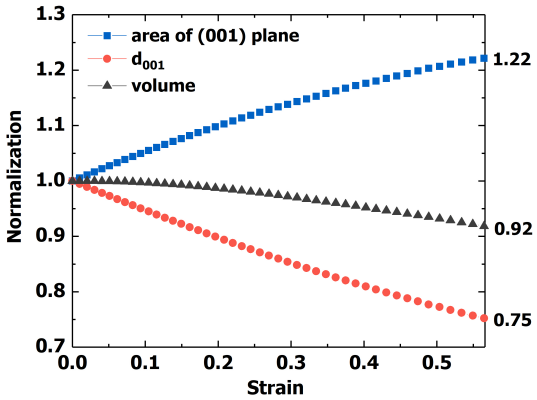

FIG. S3: The evolution of normalized (to the values of the unstrained crystal) lattice spacing between the (001) planes (d_{001}), the unit-cell area of the (001) plane and the unit-cell volume of Si under the (111)[11-2] PS strains. In the tetrahedrally bonded environment of Si crystal lattice, each Si atom has a large void site aligned opposite to one of its nearest-neighbor atoms [22]. The void positions and Si atom positions can be viewed as two face-center-cubic sublattices in the crystal structure. Under large deformations, such as the (111)[11-2] PS strains, a large angular expansion mode along with relatively small bond elongations causes a prominent contraction of the lattice spacing between the (001) planes, which is steeper than the expansion of the area of the (001) planes, leading to the reduced volume of the void, and thus an overall reduction of volume for the deformed crystal.

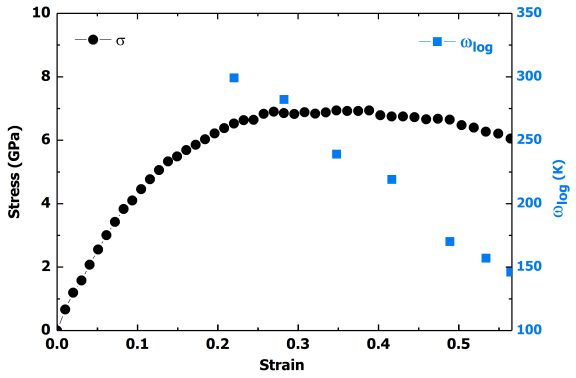

FIG. S4: Calculated logarithmic average phonon frequencies as a function of strain for Si under the (111)[11-2] PS deformation mode. There is a clear relation between the flattening of the stress-strain curve, which reflects the weakening of the bonding interaction in the deformed crystal, and a sharp and steady decline of the logarithmic average phonon frequencies in the (super)conducting phase of Si.

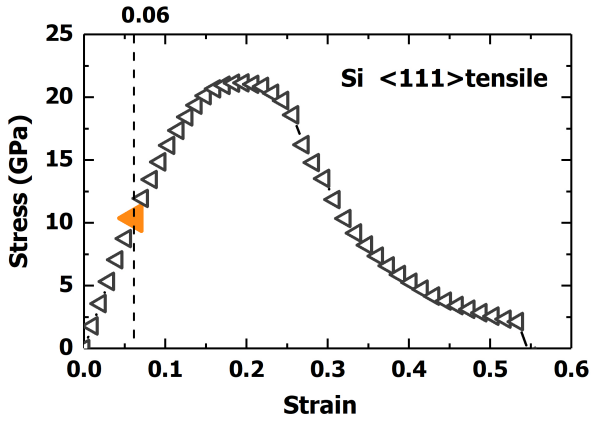

FIG. S5: Stress response of Si under (111) tensile strain. A point at 6% strain with a stress of 10 GPa near the middle of the elastic range, is selected as a representative condition for the evaluation of Si under the TS (111)[11-2] strains.

cent study shows that Si and diamond have the lowest degree of anharmonicity among all the crystals [14]. SiC involves the same two elements in the same crystal structure and is therefore expected to possess a similarly low level of degree of anharmonicity. Further, recent experiments demonstrated that nearly defect-free silicon and diamond nanostructures can approach theoretical strain and stress limits [15–20]. These studies show that achieving theoretically predicted large structural deformation is feasible. Overall, we expect that anharmonic effects will not have any appreciable impact on the main conclusions of our reported work.

Previous research revealed that anharmonic effect

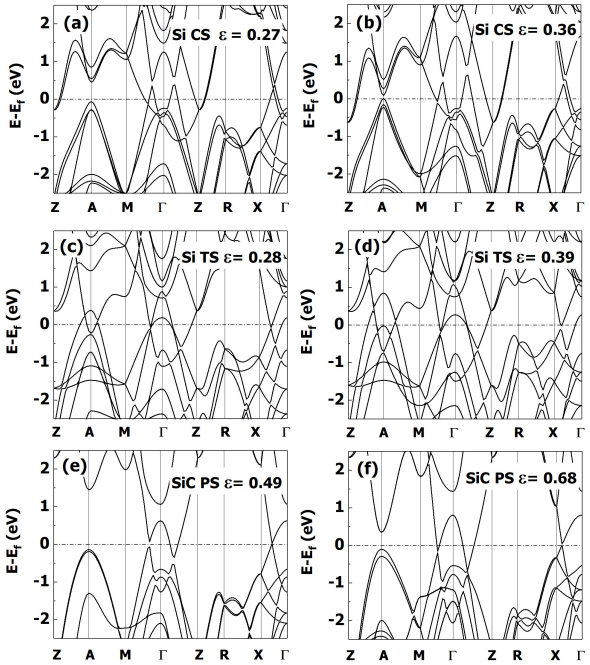

FIG. S6: Electronic band structures of (a, b) Si under the (11-2)[111] CS strains, (c, d) Si under the (111)[11-2] TS strains, and (e, f) SiC under the (111)[11-2] PS strains. These results show clear trends of shear strain driven increase of band crossing at the Fermi level, similar to the results for Si under the (111)[11-2] PS strains shown in Figs. 2(c) and 2(d).

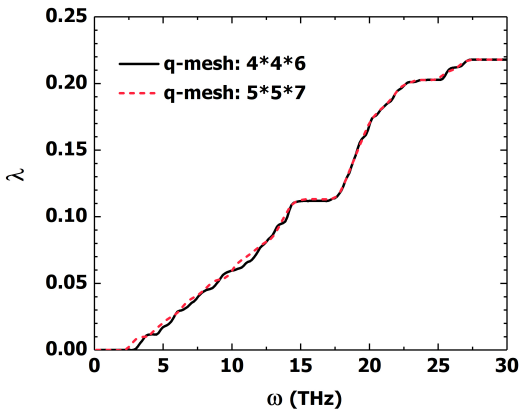

FIG. S7: Mesh convergence test for the calculated coupling integral $\lambda(\omega)$ at selected PS strain of 0.49 in deformed SiC. An 8-atoms cell is used in the calculations for electron-phonon coupling parameter. The calculated coupling integral $\lambda(\omega)$ at ϵ=0.49 with 4×4×6 and 5×5×7 q mesh generates 34 and 54 irreducible q points, respectively. The calculations with the distinct q-mesh choices yield nearly identical integrated λ values and Tc values, confirming that the q-mesh of 4×4×6 used in the present work is adequate to provide a reliable description for the phonon-mediated superconductivity.

could eliminate imaginary phonon modes and stabilize crystal structure that is dynamically unstable according to phonon calculations under harmonic approximation [21]. Such effects could impact structural stability of crystals under large strains, possibly leading to increased strain range and enhanced physical properties such as metallicity and superconductivity, especially in materials that host large anharmonicity. Further investigationsare required for a full understanding of this important and intricate topic.

* Electronic address: liquan777@calypso.cn
† Electronic address: mym@jlu.edu.cn
‡ Electronic address: chen@physics.unlv.edu

[1] G. Kresse and L. Furthmüller, Efficient Iterative Schemes for Ab initio Total-Energy Calculations Using a Plane-Wave Basis Set. Phys. Rev. B **54**, 11169 (1996).
[2] G. Kresse and D. Joubert, From Ultrasoft Pseudopotentials to the Projector Augmented-Wave Method. Phys. Rev. B **59**, 1758 (1999).
[3] D. M. Ceperley and B. J. Alder, Ground State of the Electron Gas by a Stochastic Method. Phys. Rev. Lett. **45**, 566 (1980).
[4] H. J. Monkhorst and J. D. Pack, Special Points for Brillouin-Zone Integrations. Phys. Rev. B **13**, 5188 (1976).
[5] J. Heyd, G. E. Scuseria, and M. Ernzerhof, Hybrid Functionals Based on a Screened Coulomb Potential. J. Chem. Phys. **118**, 8207 (2003).
[6] J. Heyd, G. E. Scuseria, and M. Ernzerhof, Erratum: Hybrid Functionals Based on a Screened Coulomb Potential. J. Chem. Phys. **124**, 219906 (2006).
[7] W. Bludau, A. Onton, and W. Heinke, Temperature dependence of the band gap of silicon, J. Appl. Phys. **45**, 1846 (1974).
[8] R. G. Humphreys, D. Bimberg, and W. J. Choyke, Wavelength modulated absorption in SiC, Solid State Commun. **39**, 163 (1981).
[9] Z. C. Pan, H. Sun, and C. F. Chen, Colossal shear-strength enhancement of lowdensity cubic BC_2N by nanoindentation. Phys. Rev. Lett. **98**, 135505 (2007).
[10] Z. C. Pan, H. Sun, Y. Zhang, and C. F. Chen, Harder than diamond: superior indentation strength of wurtzite BN and lonsdaleite. Phys. Rev. Lett. **102**, 1055503 (2009).
[11] B. Li, H. Sun, and C. F. Chen, Large indentation strain stiffening in nanotwinned cubic boron nitride. Nat. Commun. **5**, 4965 (2014).
[12] P. Giannozzi et al., QUANTUM ESPRESSO: a modular and open-source software project for quantum simulations of materials, J. Phys. Condens. Matter **21**, 395502 (2009).
[13] J. C. Thomas and A. Van der Ven, Finite-temperature properties of strongly anharmonic and mechanically unstable crystal phases from first principles, Phys. Rev. B **88**, 214111 (2013).
[14] F. Knoop, T. A. R. Purcell, M. Scheffler, and C. Carbogno, Anharmonicity measure for materials, Phys. Rev. Matter. **4**, 083809 (2020).
[15] H. Zhang, J. Tersoff, S. Xu1, H. Chen, Q. Zhang, K. Zhang, Y. Yang, C.-S. Lee, K.-N. Tu, J. Li, and Y. Lu, Approaching the ideal elastic strain limit in silicon nanowires, Sci. Adv. **2**, e1501382 (2016).
[16] A. Banerjee, D. Bernoulli, H. Zhang1, M. F. Yuen, J. Liu, J. Dong, F. Ding, J. Lu, M. Dao, W. Zhang, Y. Lu, S. Suresh, Ultralarge elastic deformation of nanoscale diamond, Science **360**, 300 (2018).
[17] A. Nie, Y. Bu, P. Li, Y. Zhang, T. Jin, J. Liu, Z. Su, Y. Wang, J. He, Z. Liu, H. Wang, Y. Tian, and W. Yang, Approaching diamond担theoretical elasticity and strength limits, Nat. Commun. **10**, 5533 (2019).
[18] M. Chen, L. Pethö, A. S. Sologubenko, H. Ma, J. Michler, R. Spolenak, and J. M. Wheeler, Achieving micron-scale plasticity and theoretical strength in Silicon, Nat. Commun. **11**, 2681 (2020).
[19] Z. Shi, M. Dao, E. Tsymbalov, A. Shapeev, J. Li, and S. Suresh, Metallization of diamond, Proc. Natl. Acad. Sci. (USA) **117**, 24634 (2020).
[20] C. Dang, J. Chou, B. Dai, C. Chou, Y. Yang, R. Fan, W. Lin, F. Meng, A. Hu, J. Zhu, J. Han, A. M. Minor, J. Li, Y.Lu, Achieving large uniform tensile elasticity in microfabricated diamond, Science **371**, 76 (2021).
[21] I. Errea, M. Calandra, C. J. Pickard, J. R. Nelson, R. J. Needs, Y. Li, H. Liu, Y. Zhang, Y. Ma, and F. Mauri, Quantum hydrogen-bond symmetrization in the superconducting hydrogen sulfide system, Nature **532**, 81 (2016).
[22] G. Shen, D. Ikuta, S. Sinogeikin, Q. Li, Y. Zhang, and C. F. Chen, Direct Observation of a Pressure-Induced Precursor Lattice in Silicon, Phys. Rev. Lett. **109**, 205503 (2012).